Ti$_4$Ir$_2$O: A time reversal invariant fully gapped unconventional superconductor

Debarchan Das,[1] KeYuan Ma,[2] Jan Jaroszynski,[3] Vahid Sazgari,[1] Tomasz Klimczuk,[4,5]
Fabian O. von Rohr,[6,*] and Zurab Guguchia[1,†]

[1]*PSI Center for Neutron and Muon Sciences CNM, 5232 Villigen PSI, Switzerland*
[2]*Max Planck Institute for Chemical Physics of Solids, 01187 Dresden, Germany*
[3]*National High Magnetic Field Laboratory, Florida State University, Tallahassee, Florida 32310, USA*
[4]*Faculty of Applied Physics and Mathematics, Gdansk University of Technology, ul. Narutowicza 11/12, Gdańsk 80–233, Poland*
[5]*Advanced Materials Centre, Gdansk University of Technology, ul. Narutowicza 11/12, Gdańsk 80–233, Poland*
[6]*Department of Quantum Matter Physics, University of Geneva, CH-1211 Geneva, Switzerland*

Here we report muon spin rotation (μSR) experiments on the temperature and field dependence of the effective magnetic penetration depth $\lambda(T)$ in the η-carbide-type suboxide Ti$_4$Ir$_2$O, a superconductor with a considerably high upper critical field. The temperature dependence of $\lambda(T)$, obtained from transverse-field (TF)-μSR measurements, is in perfect agreement with an isotropic fully gaped superconducting state. Furthermore, our ZF μSR results confirm that the time-reversal symmetry is preserved in the superconducting state. We find, however, a remarkably small ratio of $T_c/\lambda_0^{-2} \sim 1.22$. This value is close to most unconventional superconductors, showing that a very small superfluid density is present in the superconducting state of Ti$_4$Ir$_2$O. The presented results will pave the way for further theoretical and experimental investigations to obtain a microscopic understanding of the origin of such a high upper critical field in an isotropic single-gap superconducting system.

The quest for superconducting materials for groundbreaking applications continues to drive the condensed matter research community, leading to the discovery of an array of novel superconductors and improved superconducting properties [1]. Much research effort has been put forward to advance novel superconducting materials with improved properties such as high transition temperature (T_c), high value of the critical current, and of the upper critical field (H_{c2}). Furthermore, the high upper critical fields H_{c2} are of interest from a fundamental point of view, as these are commonly associated with unconventional, possibly even topological, superconductivity [2–4]. High upper critical fields are also associated with unusual field-induced superconducting states, such as, e.g., the Fulde-Ferrell-Larkin-Ovchinnikov (FFLO) state, which is a distinct superconducting phase observed in spin-singlet superconductors [5–7].

One recent approach to control the properties of superconductors has been the chemically precise filling of the void position in the crystal structures using electron-donor atoms to chemically tune the electronic properties of these materials [8,9]. Along this line, η-carbide-type oxides turn out to be a promising material platform since it results from filling void

*Contact author: fabian.vonrohr@unige.ch
†Contact author: zurab.guguchia@psi.ch

positions in the Ti$_2$Ni-type structure, with small nonmetallic atoms such as oxygen, nitrogen, or carbon occupying the interstitial positions [15].

The η-carbide family of compounds, encompasses a variety of materials which are important for the investigation of emergent quantum properties [10–14]. Most importantly, some members of this family exhibit superconductivity [10,14,16]. One notable example is Ti$_4$Ir$_2$O, which manifests superconducting properties with a critical temperature of $T_c \simeq 5.3$ K along with a considerably high upper critical field of $\mu_0 H_{c2} \sim 16$ T as revealed from bulk measurements [10]. Interestingly, the H_{c2} exceeds the weak-coupling Pauli limit ($\mu_0 H_{\text{Pauli}} \approx 9.8$ T) which corresponds to the paramagnetic pair breaking effect governing the maximal H_{c2} in conventional superconductors [17]. Recent density functional theory (DFT) calculations revealed the presence of multiple bands crossing at the Fermi energy E_F signaling plausible multigap superconductivity in Ti$_4$Ir$_2$O. Moreover, there is a pronounced peak of the density of states close to E_F, arising from the weakly dispersing energy bands [16]. This aspect resembles a key aspect of the recently widely discussed flat-band kagome superconductors [18–21]. Most recently, it was found that Ti$_4$Ir$_2$O maybe the first fully isotropic FFLO superconductor, contrary to the previous candidates, which all display highly anisotropic layered structures [22].

To gain insight into the superconducting properties of Ti$_4$Ir$_2$O, we conducted muon spin rotation/relaxation (μSR) experiments, a technique highly sensitive to superconducting gap structures in materials [23–25]. Using transverse field (TF) μSR in type-II superconductors, we can assess the temperature dependence of the magnetic penetration depth λ,

crucial for understanding the superconducting gap structure. Additionally, zero-field (ZF) μSR is effective for detecting very small internal magnetic fields, ideal for exploring spontaneous magnetic fields related to broken time-reversal symmetry in exotic superconductors [26–32].

In this Letter, we report on the low density of Cooper pairs (dilute superfluid) and unusually high upper critical field larger than the Pauli limit in η-carbide-type suboxide Ti_4Ir_2O. We, furthermore, demonstrate the isotropic fully gap pairing and the preserved time-reversal symmetry in the SC state of this system. These results identify Ti_4Ir_2O as a time-reversal-invariant fully gapped unconventional superconductor.

Polycrystalline Ti_4Ir_2O samples were synthesized from high-purity titanium (purity: 99.9%, Alfa Aesar), iridium (purity: 99.99%, Strem Chemicals), and titanium dioxide powders (purity: 99.9%, Sigma-Aldrich) via arc-melting and solid-state reaction. Initially, the reactants were mixed in stoichiometric ratios, formed into a pellet, and melted in an arc furnace under a purified argon atmosphere to ensure homogeneity. The resulting melt was then ground into fine powders, repelletized, and annealed in a sealed quartz tube at $1000°$ C for 7 days under a partial argon atmosphere. The reaction was completed by cooling the quartz tube to room temperature through water quenching.

For magnetotransport measurements, a bar-shaped sample was used with four 50-μm dia platinum wire leads spark-welded to the sample surface. The transport measurements were performed in the 35-T resistive magnet at the National High Magnetic Field Laboratory. The magnet was swept from 11.5 T to 20 T owing to the static 11.5 T background field generated by the outer superconducting coil of the magnet combination. The temperature under 2 Kelvin was ascertained using the vapor pressure of Helium-3, which remains unaffected by magnetic fields. This method contrasts with the use of Cernox and Ruthenium Oxide thermometers, which exhibit significant magnetoresistance. Transport measurements in lower fields were performed using a Physical Properties Measurements System (PPMS) from Quantum Design, equipped with a 9T superconducting magnet.

Transverse-field (TF) and zero-field (ZF) μSR experiments were carried out at the $\pi E1$ beamline on the DOLLY spectrometer at the Paul Scherrer Institute (Villigen, Switzerland). The field-dependent TF-μSR experiments at 1.6 K were were performed at $\pi M3.2$ beamline using the General Purpose Surface-Muon Instrument (GPS) spectrometer. For μSR experiments, we used a powdered sample which was pressed into a 7-mm pellet and then mounted on a Cu holder using GE varnish. This holder assembly was then mounted in the respective spectrometer cryostat. Both spectrometers are equipped with a standard veto setup [33] providing a low-background μSR signal. All the TF experiments were performed after field-cooled-cooling the sample. The μSR time spectra were analyzed using the MUSRFIT software package [34].

Ti_4Ir_2O crystallizes in the η-carbide type structure in the cubic space group $Fd\bar{3}m$, with a unit cell parameter of $a = 11.62931(2)$ Å at room temperature [10]. In Fig. 1(a), we show a schematic view of the Ti_4Ir_2O crystal structure along two orientations. The number of atoms in the unit cell is 112, of which 96 are metal atoms and 16 are oxygen. In the structure, titanium atoms occupy the 16c and the 48f Wyckoff
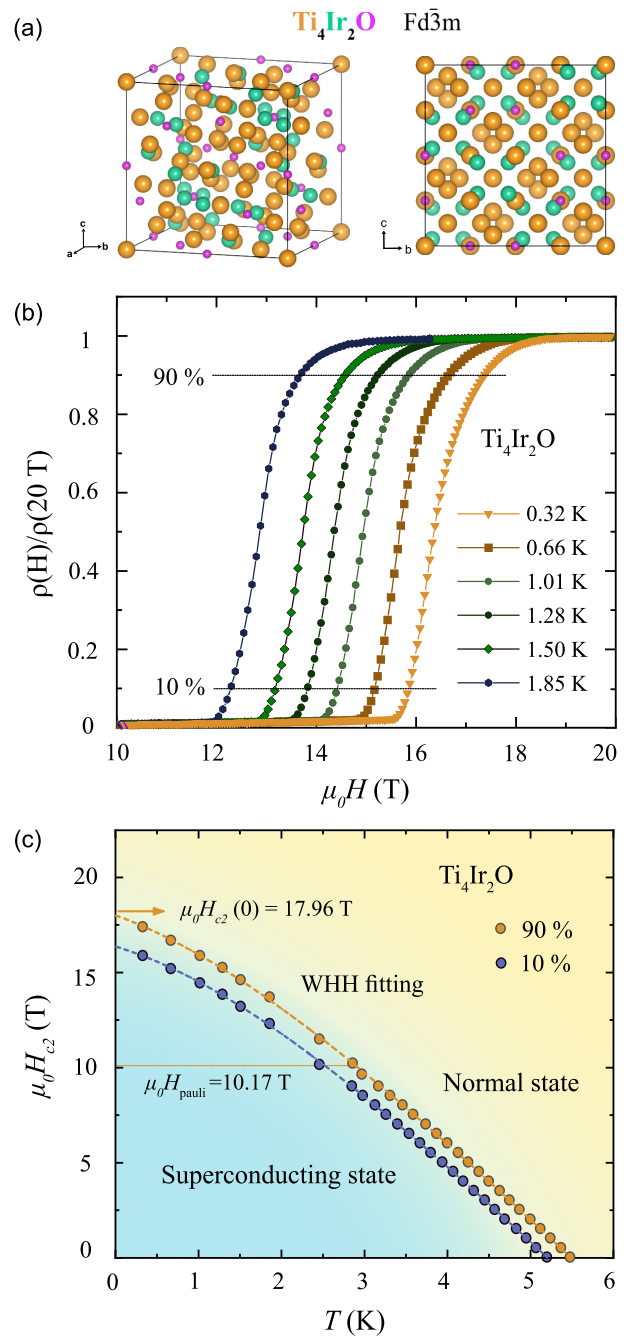

FIG. 1. (a) Schematic representation of two orientations for the crystal structure of Ti_4Ir_2O, (b) high magnetic field (10 to 20 T) transport measurement of Ti_4Ir_2O at low temperatures down to 300 mK (c) $\mu_0H_{c2}(T)$ phase diagram of Ti_4Ir_2O determined from electrical transport measurements under external fields.

positions, iridium atoms occupy the 32e Wyckoff positions, and oxygen atoms occupy the 16d Wyckoff positions, resulting in a formula of $Ti_{64}Ir_{32}O_{16}$ for one unit cell [10]. The prepared polycrystalline Ti_4Ir_2O samples were found to be single phase by means of powder x-ray diffraction measurement.

In Fig. 1(b), we present high magnetic field (20 T) transport measurement of Ti_4Ir_2O down to 320 mK. The data were plot as the normalized resistivity $\rho(H)/\rho(20$ T) versus

magnetic field μ_0H(T) at different constant below the critical temperature T_{rmc}. We can clearly observe the transition to the normal state from the superconducting state at high magnetic fields under all measured temperatures. Here, we determined the superconducting transition critical field μ_0H(T) at different temperatures by the 10% and 90% criteria as shown in Fig. 1(b). We utilized both criteria to estimate the critical field due to the slightly broad nature of the transition. These high magnetic field transport measurement data together with those measured under lower fields (below 9 T) were used to obtain the upper critical field $\mu_0H_{c2}(0)$ as shown in Fig. 1(c).

The upper critical field $\mu_0H_{c2}(0)$ of Ti$_4$Ir$_2$O was estimated using the Werthamer-Helfand-Hohenberg (WHH) approximation in the clean limit [10]

$$\mu_0H_{c2}(T) = \frac{\mu_0H_{c2}(0)}{0.73}h^*_{\text{fit}}(T/T_c), \tag{1}$$

$$h^*_{\text{fit}}(t) = (1-t) - C_1(1-t)^2 - C_2(1-t)^4, \tag{2}$$

where $t = T/T_c$ and T_c is the transition temperature at zero magnetic field. In Fig. 1(c), we show the $\mu_0H_{c2}(0)$ fitting of Ti$_4$Ir$_2$O using the Werthamer-Helfand-Hohenberg (WHH) approximation in the clean limit. We found the fitting lines well describe all the obtained experimental points, and the narrow space between the 90%- and 10%-fitting lines suggests the superconducting transition width of Ti$_4$Ir$_2$O is small. The $\mu_0H_{c2}(0)$ values were determined to be 17.96 T and 16.32 T for the 90% and 10% criteria, respectively. These values are exceeding by far than the corresponding Pauli paramagnetic limit μ_0H_{Pauli} of 10.17 T and 9.65 T, which are derived from $\mu_0H_{\text{Pauli}} \approx 1.86[\text{T/K}] \cdot T_c$ for a weak-coupling Bardeen-Cooper-Schrieffer (BCS) superconductor. Here, this unusually high upper critical field indicates an unconventional superconductivity behavior in Ti$_4$Ir$_2$O.

Figure 2(a) shows TF-μSR spectra for Ti$_4$Ir$_2$O measured in an applied magnetic field of 30 mT at temperatures above (7 K) and below (0.27 K) the critical temperature T_c. A small relaxation, observed in TF-μSR spectra above T_c, can be attributed to the presence of random local fields associated with the nuclear magnetic moments. In the superconducting state, the formation of FLL creates an inhomogeneous distribution of magnetic field which leads to the increase of the relaxation rate of the μSR signal below T_c.

Magnetism, if present in the samples, may also enhance the muon depolarization rate and influence the interpretation of the TF-μSR results. Therefore, we carried out ZF-μSR experiments above and below T_c to search for magnetism (static or fluctuating) in Ti$_4$Ir$_2$O. As seen from Fig. 2(b), we do not observe any noticeable difference in ZF-μSR asymmetry spectra recorded at temperatures above and below T_c. The ZF-μSR spectra can be well described by the Gaussian Kubo-Toyabe (GKT) depolarization function [35]

$$A^{\text{GKT}}_{\text{ZF}}(t) = A_0\left(\frac{1}{3} + \frac{2}{3}(1 - \Delta^2t^2)\exp\left[-\frac{\Delta^2t^2}{2}\right]\right). \tag{3}$$

Here, Δ/γ_μ is the width of the local field distribution due to the presence of the dense system of nuclear moments. However, this Gaussian component may also include the field distribution at the muon site created by a dense network of weak electronic moments. $\gamma_\mu = 0.085$ μs^{-1}G^{-1} is the
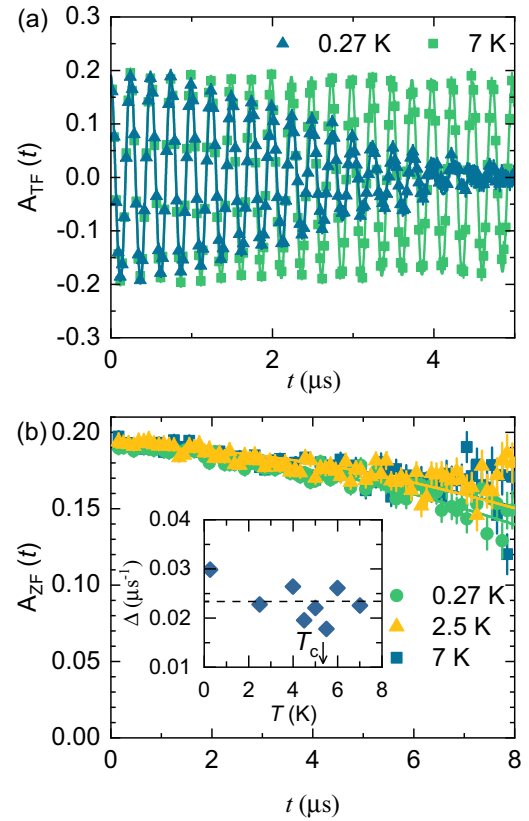

FIG. 2. (a) TF μSR time domain spectra obtained above and below T_c for Ti$_4$Ir$_2$O in an applied field of 30 mT (after field cooling the sample from above T_c). (b) ZF μSR asymmetry spectra recorded at 0.27 and 7 K for Ti$_4$Ir$_2$O. Inset: Temperature dependence of the electronic relaxation rate measured in zero magnetic field. The error bars are smaller than the data points.

muon gyromagnetic ratio. The inset of Fig. 2(b) shows the temperature evolution of Δ, which shows no noticeable enhancement across T_c. The initial asymmetry was also found to be temperature independent and remained constant throughout the final analysis. The maximum possible spontaneous flux density due to superconductivity can be estimated using $(\Delta|_{0.27\,\text{K}} - \Delta|_{7\,\text{K}})/(2\pi\gamma_\mu) = 1.49\,\mu$T which is several times smaller than that seen for well-known TRS breaking superconductors [27,28]. This demonstrates the absence of any spontaneous field in either the normal or the superconducting state of Ti$_4$Ir$_2$O. Therefore, this sample is nonmagnetic and also the time-reversal symmetry is preserved in the superconducting state of this compound.

The absence of magnetism in Ti$_4$Ir$_2$O implies that the increase of the TF relaxation rate below T_c is attributed entirely to the flux-line lattice (FLL). Assuming a Gaussian field distribution, we analyzed the observed TF-μSR asymmetry spectra by using the following functional form:

$$A_{\text{TF}}(t) = A_0\exp(-\sigma^2t^2/2)\cos(\gamma_\mu B_{\text{int}}t + \varphi), \tag{4}$$

where A_0 refers to the initial asymmetry, $\gamma_\mu/2\pi \simeq 135.5$ MHz/T is the muon gyromagnetic ratio, and φ is the initial phase of the muon-spin ensemble, B_{int} corresponds to the internal magnetic field at the muon site, respectively, and σ is
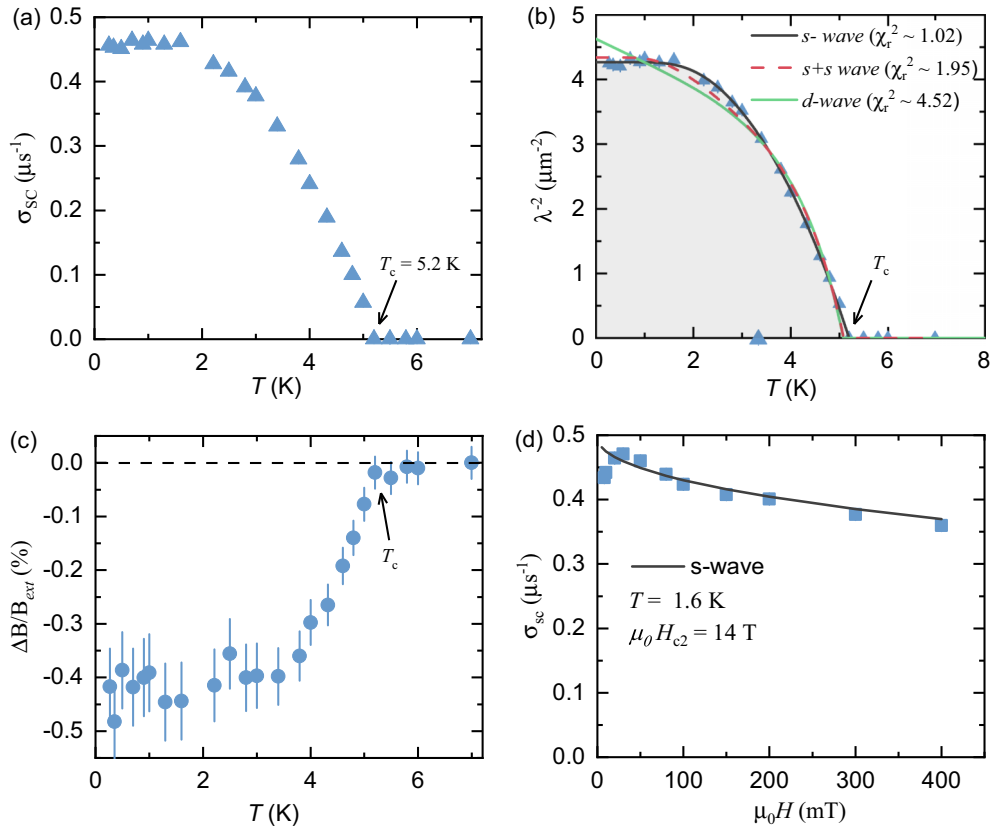
FIG. 3. (a) Temperature evolution of the superconducting muon spin depolarization rate σ_{sc} of Ti_4Ir_2O measured in an applied magnetic field of 30 mT. (b) Temperature evolution of $\lambda^{-2}(T)$ measured in an applied field $\mu_0H = 30$ mT. The solid and dashed lines represent fitting with different theoretical models as discussed in the text. For $s + s$-wave fitting, we fixed the gap values obtained from heat capacity data [16]. (c) Temperature dependence of the relative change of the internal field normalized to the external applied field, $\Delta B/B_{ext}(= \frac{B_{int}-B_{ext}}{B_{ext}})$. (d) The field dependence of TF relaxation rate $\sigma_{sc}(B)$ measured at 1.6 K.

the total relaxation rate. σ is correlated to the superconducting relaxation rate σ_{SC}, following the relation $\sigma = \sqrt{\sigma_{nm}^2 + \sigma_{SC}^2}$ where σ_{nm} is the nuclear contributions that is assumed to be temperature independent. To estimate σ_{SC}, we consider the value of σ_{nm} obtained above T_c where only nuclear magnetic moments contribute to the muon depolarization rate σ. The solid lines in Fig. 1(b) depicts the fits to the observed spectra with Eq. (4).

In Fig. 3(a), we present σ_{sc} as a function of temperature for Ti_4Ir_2O measured at an applied field of 30 mT. Below T_c, the relaxation rate σ_{sc} increases from zero due to inhomogeneous field distribution caused by the formation of FLL, and saturates at low temperatures. In the following section, we show that the observed temperature dependence of σ_{sc}, which reflects the topology of the superconducting gap, is consistent with the presence of the single gap on the Fermi surface of Ti_4Ir_2O. Figure 3(c) shows the temperature dependence of the relative change of the internal field normalized to the external applied field, $\Delta B/B_{ext}(= \frac{B_{int}-B_{ext}}{B_{ext}})$. As seen from the figure, internal field values in the superconducting state, i.e., $(T < T_c)$ are lower than the applied field because of the diamagnetic shift, expected for type-II superconductors.

For a perfect triangular vortex lattice, $\sigma_{sc}(T)$ is directly related to the London magnetic penetration depth $\lambda(T)$ by

[36,37]

$$\frac{\sigma_{sc}^2(T)}{\gamma_\mu^2} = 0.00371\frac{\Phi_0^2}{\lambda^4(T)}, \quad (5)$$

where $\Phi_0 = 2.068 \times 10^{-15}$ Wb is the magnetic flux quantum. It is important to note that Eq. (5) is valid when the separation between the vortices is smaller than λ [36]. We analyze the temperature dependence of the magnetic penetration depth, $\lambda^{-2}(T)$ to unveil the superconducting gap structure of Ti_4Ir_2O.

Within the London approximation $(\lambda \gg \xi)$, $\lambda(T)$ can be described by the following expression [17,34,38]:

$$\frac{\lambda^{-2}(T, \Delta_{0,i})}{\lambda^{-2}(0, \Delta_{0,i})} = 1 + \frac{1}{\pi}\int_0^{2\pi}\int_{\Delta(T,\varphi)}^\infty \left(\frac{\partial f}{\partial E}\right)\frac{E dE}{\sqrt{E^2 - \Delta_i(T,\varphi)^2}}, \quad (6)$$

where $f = [1 + \exp(E/k_B T)]^{-1}$ is the Fermi function, φ is the azimuthal angle along the Fermi surface, and $\Delta_{0,i}(T) = \Delta_{0,i} \Gamma(T/T_c) g(\varphi)$. $\Delta_{0,i}$ is the maximum gap value at $T = 0$ K. The temperature dependence of the gap is described by the expression $\Gamma(T/T_c) = \tanh\{1.82[1.018(T_c/T - 1)]^{0.51}\}$ [39]. For the s-wave gap and a nodal d-wave, the angular dependence $g(\varphi)$ corresponds to 1 and $|\cos(2\varphi)|$, respectively. We consider three models in our analysis: (i) an isotropic s-wave

gap; (ii) a combination of two s-wave gaps of different size; and (iii) a nodal d wave model.

As seen from Fig. 3(b), the experimentally obtained $\lambda^{-2}(T)$ dependence can be best described using a single s-wave model yielding a gap value of $\Delta_0 = 0.92(8)$ meV and $T_c = 5.19(3)$ K. Previously from heat capacity analysis, Ruan *et al.* [16] predicted the presence of two superconducting gaps ($\Delta_{0,1} = 1.37$ meV and $\Delta_{0,2} = 0.57$ meV). Therefore, to test this possible multigap scenario, we use these gap values and kept them fixed in our analysis.

For the two-gap scenario, we use the weighted sum of two gaps

$$\frac{\lambda^{-2}(T)}{\lambda^{-2}(0)} = x\frac{\lambda^{-2}(T, \Delta_{0,1})}{\lambda^{-2}(0, \Delta_{0,1})} + (1 - x)\frac{\lambda^{-2}(T, \Delta_{0,2})}{\lambda^{-2}(0, \Delta_{0,2})}. \quad (7)$$

Here x is the weight associated with the larger gap and $\Delta_{0,i}$ ($i = 1, 2$ are the gap indices) are the gaps.

A close look at the goodness of fit suggests that the single s-wave model gives the lowest value of χ_r^2 indicates the best fit to the observed data. We note that while fitting the experimental data keeping two gaps as free parameters, the weight of the higher gap (x) reaches a value close to 0, implying the single-gap scenario is more appropriate. Also the d-wave gap symmetry was tested, but are found to be inconsistent with the data [for example, see the green solid line in Fig. 3(b)]. Thus, from the μSR experiments, we confirm the presence of a single fully-gapped superconducting state in Ti$_4$Ir$_2$O.

We also investigate the field dependence of the TF-relaxation rate $\sigma_{sc}(B)$ measured at 1.6 K [see Fig. 3(d)]. For these measurements, each point was obtained by field-cooling the sample from 10 K (above T_c) to 1.6 K. σ_{sc} first increases to a maximum with increasing magnetic field followed by a continuous decrease up to the highest field (400 mT) studied as expected for a single-gap superconductor with an ideal triangular vortex lattice. Interestingly, the observed $\sigma_{sc}(B)$ curve at fields above the maximum, can be well modeled by using the Brandt formula (for a single s-wave gap superconductor) [37] with an upper critical field $\mu_0 H_{c2}(0.27\,K) = 14$ T at 1.6 K.

While the temperature and field dependence of the London penetration depth λ_{eff}^{-2} and henceforth of the superfluid density can be well understood as a fully gapped s-wave superconductor, the T_c/λ_{eff}^{-2} ratio for Ti$_4$Ir$_2$O is comparable to those of unconventional superconductors [40–43]. In the context of

the Bose-Einstein condensation (BEC) to BCS crossover [40], systems with a small ratio of T_c/λ_{eff}^{-2} (approximately 0.00025–0.015) are categorized on the BCS-like side, indicative of conventional superconductivity. In contrast, a large ratio in the range of 1–20, along with a linear relationship between T_c and λ_{eff}^{-2}, is typically observed on the BEC-like side, signifying unconventional superconductivity. This framework has been historically utilized to differentiate between BCS-like (conventional) and BEC-like (unconventional) superconductors. The results obtained for Ti$_4$Ir$_2$O show a ratio of $T_c/\lambda_{eff}^{-2} \simeq 1.22$, closely aligning with the ratio of approximately 1 seen in electron-doped cuprates. This finding, alongside previously reported high upper critical fields and thermodynamic evidence of an FFLO state, provides strong support for an unconventional pairing mechanism in Ti$_4$Ir$_2$O.

In conclusion, we provide the first microscopic investigation of superconductivity in the η-carbide-type suboxide Ti$_4$Ir$_2$O with a bulk probe. Namely, the zero-temperature magnetic penetration depth $\lambda_{eff}(0)$ and the temperature as well as the field dependence of λ_{eff}^{-2} were studied by means of μSR experiments.

We demonstrated the isotropic fully gap pairing and the preserved time-reversal symmetry in the SC state of this material. Interestingly, the T_c/λ_{eff}^{-2} ratio is comparable to those of high-temperature unconventional superconductors, pointing to the unconventional nature of superconductivity in Ti$_4$Ir$_2$O. This result, together with earlier findings of the high upper critical field larger than the Pauli limit and the thermodynamic signatures for an FFLO state, hints towards an unconventional pairing mechanism in this material. These results identify Ti$_4$Ir$_2$O as time-reversal-invariant fully gapped unconventional superconductor.

[1] X. Zhou, W.-S. Lee, M. Imada, N. Trivedi, P. Phillips, H.-Y. Kee, P. Törmä, and M. Eremets, High-temperature superconductivity, Nat. Rev. Phys. **3**, 462 (2021).

[2] J. Falson, J. Y. Xu, M. Liao, Y. Zang, K. Zhu, C. Wang, Z. Zhang, H. Liu, W. Duan, K. He, H. Liu, J. H. Smet, D. Zhang, and Q.-K. Xue, Type-II Ising pairing in few-layer stanene, Science **367**, 1454 (2020).

[3] S. Khim, J. F. Landaeta, J. Banda, N. Bannor, M. Brando, P. M. R. Brydon, D. Hafner, R. Küchler, R. Cardoso-Gil, U. Stockert, A. P. Mackenzie, D. F. Agterberg, C. Geibel, and E. Hassinger, Field-induced transition within the superconducting state of CeRh$_2$As$_2$, Science **373**, 1012 (2021).

[4] F. O. von Rohr, Chemical principles of intrinsic topological superconductors, Chem. Mater. **35**, 9455 (2023).

[5] P. Fulde and R. A. Ferrell, Superconductivity in a strong spin-exchange field, Phys. Rev. **135**, A550 (1964).

[6] A. I. Larkin, Y. N. Ovchinnikov, Nonuniform state of superconductors, Zh. Eksp. Teor. Fiz. **47**, 1136 (1964).

[7] A. K. Clogston, Upper limit for the critical field in hard superconductors, Phys. Rev. Lett. **9**, 266 (1962).

[8] Y. Zhang, B. Wang, Z. Xiao, Y. Lu, T. Kamiya, Y. Uwatoko, H. Kageyama, and H. Hosono, Electride and superconductivity behaviors in Mn$_5$Si$_3$-type intermetallics, npj Quant. Mater. **2**, 45 (2017).

[9] M. D. Balestra, O. Atanov, R. Lefèvre, O. Blacque, Y. H. Ng, R. Lortz, and F. O. von Rohr, Discovery of superconductivity in Nb_4SiSb_2 with a V_4SiSb_2-type structure and implications of interstitial doping on its physical properties, J. Mater. Chem. C **10**, 11703 (2022).

[10] K. Ma, R. Lefevre, K. Gornicka, H. O. Jeschke, X. Zhang, Z. Guguchia, T. Klimczuk, and F. O. von Rohr, Group-9 transition-metal suboxides adopting the filled-Ti_2Ni structure: A class of superconductors exhibiting exceptionally high upper critical fields, Chem. Mater. **33**, 8722 (2021).

[11] K. Ma, J. Lago, and F. V. von Rohr, Superconductivity in the η-carbide-type oxides $Zr_4Rh_2O_x$, J. Alloys Compd. **796**, 287 (2019).

[12] H. C. Ku and D. C. Johnston, New superconducting ternary transition metal compounds with the E93-type structure, Chin. J. Phys. **22**, 59 (1984).

[13] T. Waki, S. Terazawa, T. Yamazaki, Y. Tabata, K. Sato, A. Kondo, K. Kindo, M. Yokoyama, Y. Takahashi, and H. Nakamura, Interplay between quantum criticality and geometric frustration in Fe_3Mo_3N with stella quadrangula lattice, Europhys. Lett. **94**, 37004 (2011).

[14] K. Ma, K. Gornicka, R. Lefevre, Y. Yang, H. M. Ronnow, H. O. Jeschke, T. Klimczuk, and F O. von Rohr, Superconductivity with high upper critical field in the cubic centrosymmetric η-carbide $Nb_4Rh_2C_{1-\delta}$, ACS Mater. Au **1**, 55 (2021).

[15] R. Mackay, G. J. Miller, and H. F. Franzen, New oxides of the filled-Ti_2Ni type structure, J. Alloys Compd. **204**, 109 (1994).

[16] B.-B. Ruan, M.-H. Zhou, Q.-S. Yang, Y.-D. Gu, M.-W. Ma, G.-F. Chen, and Z.-A. Ren, Superconductivity with a Violation of Pauli Limit and Evidences for Multigap in η-Carbide Type Ti_4Ir_2O, Chin. Phys. Lett. **39**, 027401 (2022).

[17] M. Tinkham, *Introduction to Superconductivity* (Krieger, Malabar, FL, 1975).

[18] M. L. Kiesel, C. Platt, and R. Thomale, Unconventional fermi surface instabilities in the kagome hubbard model, Phys. Rev. Lett. **110**, 126405 (2013).

[19] B. R. Ortiz, S. M. L. Teicher, Y. Hu, J. L. Zuo, P. M. Sarte, E. C. Schueller, A. M. Milinda Abeykoon, M. J. Krogstad, S. Rosenkranz, R. Osborn, R. Seshadri, L. Balents, J. He, and S. D. Wilson, CsV_3Sb_5: A Z_2 topological kagome metal with a superconducting ground state, Phys. Rev. Lett. **125**, 247002 (2020).

[20] C. Mielke III, D. Das, J.-X. Yin, H. Liu, R. Gupta, Y.-X. Jiang, M. Medarde, X. Wu, H. C. Lei, J. Chang, Pengcheng Dai, Q. Si, H. Miao, R. Thomale, T. Neupert, Y. Shi, R. Khasanov, M. Z. Hasan, H. Luetkens, and Z. Guguchia, Time-reversal symmetry-breaking charge order in a kagome superconductor, Nature (London) **602**, 245 (2022).

[21] Z. Guguchia, R. Khasanov, and H. Luetkens, Unconventional charge order and superconductivity in kagome-lattice systems as seen by muon-spin rotation, npj Quantum Mater. **8**, 41 (2023).

[22] J. Hu *et al.*, Thermodynamic evidence for the Fulde-Ferrell-Larkin Ovchinnikov state in the isotropic superconductor Ti_4Ir_2O. arXiv:2312.01914.

[23] J. E. Sonier, J. H. Brewer, and R. F. Kiefl, μSR studies of the vortex state in type-II superconductors, Rev. Mod. Phys. **72**, 769 (2000).

[24] S. Blundell, R. De Renzi, T. Lancaster, and F. Pratt, *Introduction to Muon Spectroscopy* (Oxford University Press, New York, 2021).

[25] A. D. Hillier, S. J. Blundell, I. McKenzie, I. Umegaki, L. Shu, J. A. Wright, T. Prokscha, F. Bert, K. Shimomura, A. Berlie, H. Alberto, and I. Watanabe, Muon spin spectroscopy, Nat. Rev. Methods Primers **2**, 4 (2022).

[26] Z. Guguchia *et al.*, Tunable unconventional kagome superconductivity in charge ordered RbV_3Sb_5 and KV_3Sb_5, Nat. Commun. **14**, 153 (2023).

[27] G. M. Luke, Y. Fudamoto, K. M. Kojima, M. I. Larkin, J. Merrin, B. Nachumi, Y. J. Uemura, Y. Maeno, Z. Q. Mao, Y. Mori, H. Nakamura, and M. Sigrist, Time-reversal symmetry-breaking superconductivity in Sr_2RuO_4, Nature (London) **394**, 558 (1998).

[28] A. D. Hillier, J. Quintanilla, and R. Cywinski, Evidence for time-reversal symmetry breaking in the noncentrosymmetric superconductor $LaNiC_2$, Phys. Rev. Lett. **105**, 229901(E) (2010).

[29] J. A. T. Barker, D. Singh, A. Thamizhavel, A. D. Hillier, M. R. Lees, G. Balakrishnan, D. M. Paul, and R. P. Singh, Unconventional superconductivity in La_7Ir_3 revealed by muon spin relaxation: Introducing a new family of noncentrosymmetric superconductor that breaks time-reversal symmetry, Phys. Rev. Lett. **115**, 267001 (2015).

[30] R. P. Singh, A. D. Hillier, B. Mazidian, J. Quintanilla, J. F. Annett, D. McK Paul, G. Balakrishnan, and M. R. Lees, Detection of time-reversal symmetry breaking in the noncentrosymmetric superconductor Re_6?zr using muon-spin spectroscopy, Phys. Rev. Lett. **112**, 107002 (2014).

[31] T. Shang, M. Smidman, S. K. Ghosh, C. Baines, L. J. Chang, D. J. Gawryluk, J. A. T. Barker, R. P. Singh, D. M. Paul, G. Balakrishnan, E. Pomjakushina, M. Shi, M. Medarde, A. D. Hillier, H. Q. Yuan, J. Quintanilla, J. Mesot, and T. Shiroka, Time-Reversal symmetry breaking in re-based superconductors, Phys. Rev. Lett. **121**, 257002 (2018).

[32] P. K. Biswas, H. Luetkens, T. Neupert, T. Stürzer, C. Baines, G. Pascua, A. P. Schnyder, M. H. Fischer, J. Goryo, M. R. Lees, H. Maeter, F. Brückner, H.-H. Klauss, M. Nicklas, P. J. Baker, A. D. Hillier, M. Sigrist, A. Amato, and D. Johrendt, Evidence for superconductivity with broken time-reversal symmetry in locally noncentrosymmetric $SrPtAs$, Phys. Rev. B **87**, 180503(R) (2013).

[33] A. Amato, H. Luetkens, K. Sedlak, A. Stoykov, R. Scheuermann, M. Elender, A. Raselli, and D. Graf, The new versatile general purpose surface-muon instrument (GPS) based on silicon photomultipliers for μSR measurements on a continuous-wave beam, Rev. Sci. Inst. **88**, 093301 (2017).

[34] A. Suter and B. Wojek, Musrfit: A Free Platform-Independent Framework for μSR Data Analysis, Phys. Procedia **30**, 69 (2012).

[35] R. Kubo and T. Toyabe, *Magnetic Resonance and Relaxation* (North Holland, Amsterdam, 1967).

[36] E. H. Brandt, Flux distribution and penetration depth measured by muon spin rotation in high-T_c superconductors, Phys. Rev. B **37**, 2349 (1988).

[37] E. H. Brandt, Properties of the ideal Ginzburg-Landau vortex lattice, Phys. Rev. B **68**, 054506 (2003).

[38] R. Prozorov and R. W. Giannetta, Magnetic penetration depth in unconventional superconductors, Supercond. Sci. Technol. **19**, R41 (2006).

[39] A. Carrington and F. Manzano, Magnetic penetration depth of MgB$_2$, Physica C **385**, 205 (2003).

[40] Y. J. Uemura *et al.*, Basic similarities among cuprate, bismuthate, organic, chevrel phase, and heavy-fermion superconductors shown by penetration depth measurements, Phys. Rev. Lett. **66**, 2665 (1991).

[41] Z. Guguchia, F. von Rohr, Z. Shermadini, A. T. Lee, S. Banerjee, A. R. Wieteska, C. A. Marianetti, B. A. Frandsen, H. Luetkens, Z. Gong, S. C. Cheung, C. Baines, A. Shengelaya, G. Taniashvili, A. N. Pasupathy, E. Morenzoni, S. J. L. Billinge, A. Amato, R. J. Cava, R. Khasanov, and Y. J. Uemura, Signatures of the topological s^{+-} superconducting order parameter in the type-II Weyl semimetal T_d-MoTe$_2$, Nat. Commun. **8**, 1082 (2017).

[42] F. O. von Rohr *et al.*, Unconventional scaling of the superfluid density with the critical temperature in transition metal dichalcogenides, Sci. Adv. **5**, eaav8465 (2019).

[43] D. Das *et al.*, Time-reversal invariant and fully gapped unconventional superconducting state in the bulk of the topological Nb$_{0.25}$Bi$_2$Se$_3$, Phys. Rev. B **102**, 134514 (2020).